

$^2\text{H}$  NMR Studies of Deuterated Polycrystalline L-Cyclo(leucine-glycine)- $\text{d}_3$

Lara Lyn Bryan  
May 5, 2000

## Contents

<b>I</b>	<b>Abstract</b> .....	<b>3</b>
<b>II</b>	<b>Introduction</b> .....	<b>4</b>
<b>III</b>	<b>Theory</b> .....	<b>6</b>
	A General NMR Theory.....	6
	B Solid State NMR of a Spin-1 Particle.....	9
<b>IV</b>	<b>Experiment</b> .....	<b>13</b>
	A Temperature-Controlled Experiments.....	13
	B Computer Simulations.....	16
	1 Four Site Model.....	17
	2 Six Site Model.....	19
	3 Twenty Site Model.....	21
<b>V</b>	<b>Results and Discussion</b> .....	<b>24</b>
	A Temperature-Controlled Experiments.....	24
	B Computer Simulations.....	27
	C Comparison of Simulations to Experimental Data.....	32
<b>VI</b>	<b>Conclusion</b> .....	<b>35</b>
<b>VII</b>	<b>References</b> .....	<b>38</b>

## I. Abstract

In previous Nuclear Magnetic Resonance spectroscopy experiments, the dynamics of polycrystalline L-cyclo(leucine-glycine)-d<sub>3</sub> were studied using relaxation time anisotropies. This previous work concluded that, in addition to the anticipated fast three-site rotation of the deuterated methyl group, a supplemental simultaneous motion was occurring. The aim of the experiments described in this thesis is to characterize this additional component of molecular motion. The secondary motion of the deuterated methyl group was hypothesized to have rates in the intermediate regime between 10<sup>2</sup> and 10<sup>8</sup> s<sup>-1</sup>. The initial stage of this project was to verify the existence of molecular motion through NMR spectroscopy experiments. Temperature-dependent quadrupole echo spectra of L-cyclo(leucine-glycine)-d<sub>3</sub> support the hypothesis that there exists additional molecular motion. The second objective of the project was to propose a suitable model for the observed motion. Using a specifically tailored program to generate simulated lineshapes, three models of dynamics, ranging from a simple four-site jump model to a complex twenty-site jump model, were tested. In addition to selecting a model for the composite motion, values for relevant parameters were also hypothesized. The two most important parameters for these experiments being the quadrupole coupling constant and the rate of motion. After numerous simulations, we found the twenty-site jump model best fit our experimental data.

## II. Introduction

Nuclear magnetic resonance (NMR) spectroscopy is a widely used non-destructive experimental technique that provides information about molecular structure and dynamics. NMR spectra are well-understood for liquid samples and are used routinely for identification and analysis, especially of organic compounds. NMR can also be used to study materials in the solid state, however structural and dynamical differences between the two states make their spectra dissimilar. Furthermore, the spectra of liquids tend to be easier to interpret, since they consist of narrow peaks at characteristic absorption frequencies, whereas solid polycrystalline materials exhibit broad absorption ranges with less well-defined characteristics. Shielding and deshielding effects in liquids are also well-quantified and easily identifiable. Therefore, for analytical purposes it is advantageous to perform NMR spectroscopy on liquid samples. NMR, however, can be used specifically to investigate the structure and dynamics of molecules in the solid state that are either not capable of being dissolved or whose conversion to the liquid phase would alter the physical properties that are to be characterized. Thus, although solid-state NMR spectroscopy proves more challenging, it can provide molecular information unattainable by other methods. Solid-state NMR spectroscopy is considerably different from the typical liquid NMR spectroscopy, especially in the acquisition and analysis procedures. [1]

In 1996, Seth C. Olsen, as part of his senior honors thesis project at The College of William and Mary, used  $^2\text{H}$  NMR to examine deuterated polycrystalline L-leucine- $\text{d}_3$  and L-cyclo(leucine-glycine)- $\text{d}_3$ . [2] In the experimental relaxation times, he expected to find evidence of the rapid rotation of the deuterated methyl group, as described by E.

Oldfield.[3] Thus, he attempted to reproduce the relaxation time,  $T_{1Q}$  and  $T_{1Z}$ , anisotropies using a computer simulation program describing a 3-site jump model. The simulations worked well for the amino acid L-leucine- $d_3$ , but the simulation results for L-cyclo(leucine-glycine)- $d_3$  did not match the experimental data. Therefore, he concluded that another simultaneous motion must be occurring. This motion lowered the observed quadrupole coupling constant (QCC) and accounted for the deviations of the experimental relaxation times from the simulated model.

The experiments described in this thesis re-examine the dynamics of polycrystalline L-cyclo(leucine-glycine)- $d_3$  using quadrupole echo line shapes. In addition, a suitable model of the composite molecular motion is being researched. Molecular motion in solids generally divides into three categories depending on the rate of the motion – the fast, the intermediate, and the slow regimes. The original work done on relaxation-time anisotropies by Olsen probed motion in the fast limit, with rates greater than  $10^8 \text{ s}^{-1}$ . This previous work seemed to indicate that the additional motion in polycrystalline L-cyclo(leucine-glycine)- $d_3$  was not occurring in the fast limit.[2] Therefore, the quadrupole echo experiment was used to investigate motion in the intermediate regime, probing rates of motion in the range between  $10^2 \text{ s}^{-1}$  and  $10^8 \text{ s}^{-1}$ . Motion in the intermediate regime is easier to investigate than motion in the fast regime because it can be probed directly through changes in the quadrupole echo spectra, requiring substantially less experimental time and fewer calculations.

### III. Theory

In explaining the basic principles guiding NMR, it is easier to start with a simpler model and then extend that model to include more complex systems. The experiments in this project belong to the second category of more complex systems for two reasons. First, as noted previously, the molecule studied in this project is in the solid-state. In addition, the deuteron, the nucleus being analyzed in the NMR spectrum, is a spin-1 particle. Therefore, the theory has been broken into two sections – first to understand how NMR works and second to specify what modifications must be made to the basic theory to account for the more complex system in the experiments described in this thesis.

#### A. General NMR Theory

To understand the basic theory behind NMR spectroscopy consider the example of the hydrogen nucleus with a spin of  $I=1/2$ , where spin is the intrinsic angular momentum of a quantum particle. (Every quantum particle has an immutable characteristic spin value. In addition, only particles with angular momentum  $I>0$ , because of their unique magnetic properties, can be detected by NMR spectroscopy.) [5] If a sample containing hydrogen nuclei is placed in an external magnetic field, the individual spin-1/2 nuclei will align either parallel or anti-parallel to the applied field. These two alignments correspond to the two possible angular momentum energy levels ( $I_z=\pm 1/2$ ) of the nucleus. (In the absence of a magnetic field, these two levels are degenerate, i.e. they have the same energy.) The nucleus aligned parallel to the field

( $I_z=+1/2$ ) is in the lower energy state, while the nucleus aligned anti-parallel ( $I_z=-1/2$ ) is in the higher energy state, as seen in Figure 1.

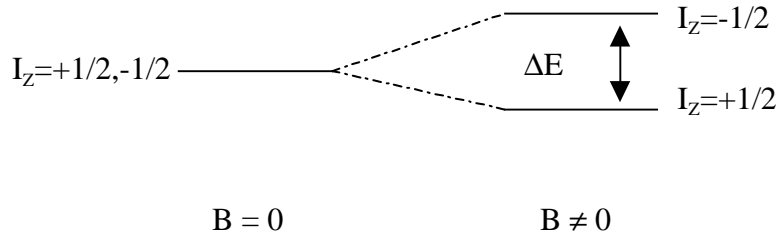


Figure 1: Energy Levels of a Spin-1/2 Particle in the Absence and in the Presence of a Static Magnetic Field.

For a nucleus of spin angular momentum  $I$ , the number of possible angular momentum energy levels is  $(2I + 1)$ , and the possible values for  $I_z$  are:

$$I_z = -I, -I+1, \dots, 0, \dots, I-1, I$$

The energy of each level is given by the equation:

$$E = - I_z h \gamma B_0$$

where  $h$  is Plank's constant,  $\gamma$  is the characteristic gyromagnetic ratio of the nucleus being studied, and  $B_0$  the strength of the external magnetic field. The energy difference between the two levels of a spin-1/2 nucleus is then:

$$\Delta E = h \gamma B_0$$

The alignment of the nuclei parallel or anti-parallel to the applied magnetic field creates a net longitudinal magnetization in the direction of the external magnetic field. In order to measure the magnetization, it needs to be perpendicular to the applied magnetic field. Thus, the equilibrium longitudinal magnetization must be converted to transverse magnetization. While the nuclei are aligned parallel and anti-parallel to the field, they are

also precessing at the Larmor frequency ( $\nu_0$ ), determined by the strength of the external magnetic field and gyromagnetic ratio, given by the equation:

$$\nu_0 = \gamma B_0$$

where  $\nu_0$  has units of Hertz.

In order to create a net transverse magnetization, a radiowave pulse is applied to the sample. When the radiowave has the same frequency as the precessing nuclei, i.e. the Larmor frequency, resonance occurs, allowing for nuclei in the ground state ( $I_z=1/2$ ) to absorb the required energy to move to the excited state ( $I_z=-1/2$ ). A nucleus makes the transition to the higher energy state by absorption of the photon. The energy of the photon absorbed is:

$$\Delta E = h \nu_{\text{photon}}$$

where  $\nu_{\text{photon}}$  is the frequency of the photon. On resonance this is the Larmor frequency,  $\nu_0$ , and the difference between two adjacent angular momentum energy levels must be:

$$\Delta E = h \nu_0$$

At resonance frequency, the radiofrequency (rf) pulse rotates the magnetization and causes the nuclei to precess in phase, resulting in the appearance of a net transverse magnetization. Immediately after the rf pulse is applied, the transverse magnetization is maximum and then decreases as the nuclei dephase with the characteristic spin-spin relaxation time  $T_2$ . A changing magnetic field induces an electric current. Therefore, the changing transverse magnetization induces an electric current in the sample coil which corresponds to the NMR signal. The NMR signal is demodulated, digitized, and stored in the computer memory as a free induction decay (FID) signal that plots magnetization as

function of time. Thus, an FID signal provides information about all the different absorption frequencies simultaneously. A more useful graph would show the various frequencies at which the nuclei absorb. This type of plot, the NMR spectrum, is obtained by Fourier Transforming the FID signal. The Fourier Transform converts the signal from the time domain to the frequency domain. In the spectrum separate peaks represent the different frequencies at which nuclei in the sample absorbed the rf pulse. Nuclei in a molecule will absorb the radiowave at different frequencies, depending on their magnetic and chemical environments: since every distinct environment corresponds to a different Larmor frequency. Therefore, the Fourier Transform NMR spectrum contains multiple peaks whenever there is more one type of magnetic or chemical nuclear environment.

### B. Solid State NMR of a Spin-1 Particle

In the experiments to be described, the nuclei being observed are deuterons which have a spin of  $I=1$ . Therefore, some modifications of the basic spin-1/2 theory are needed. Instead of two available energy levels, spin-1 particles have three distinct levels ( $I_z=-1, 0, +1$ ), as seen in Figure 2, which are degenerate when no magnetic field is present.

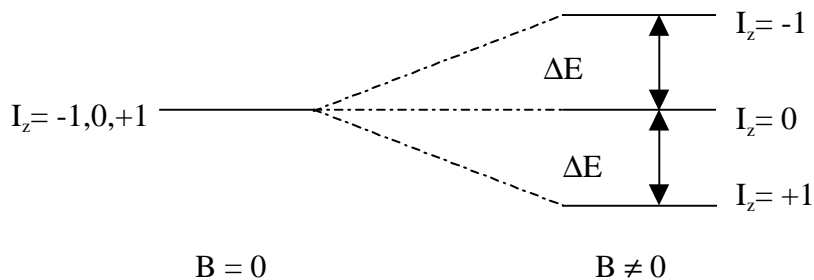


Figure 2: Energy Levels of a Spin-1 Particle in the Absence and in the Presence of a Magnetic Field.

In addition, the electric charge distribution of the nucleus is no longer spherically symmetric, giving rise to a nuclear electric quadrupole moment,  $Q$  (a parameter to measure the variation of the spin-1 charge distribution from a spherically symmetric one). The deuteron has a small quadrupole moment of approximately  $Q = 250$  kHz.[1] Because of their electric quadrupole moments, spin-1 nuclei are extremely sensitive to electric field gradients. The effect of these electric field gradients (EFG) on the quadrupole moments is called the electric quadrupole interaction. This interaction is a first order perturbation of the Zeeman angular momentum energy levels, and causes them to be unequally spaced, as seen in Figure 3.

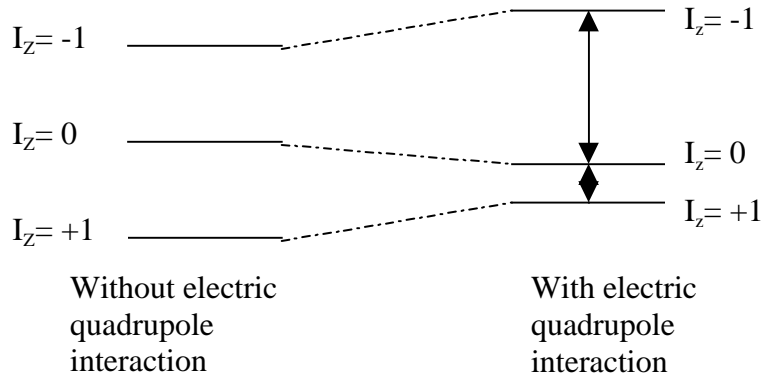


Figure 3: Energy Levels of a Spin-1 Particle in the Absence and in the Presence of Electric Quadrupole Interaction.

The Hamiltonian, correct to first order, for a system with electric quadrupole interaction

is:

$$H = -\omega_0 I_z + (1/3) \omega_Q ( 3 I_z^2 - I \cdot I )$$

where  $\omega_Q$  is defined by:

$$\omega_Q = (3\pi/4) (e^2 q_{ZZ} Q/ h ) [(3 \cos^2 \beta_{LP} - 1) + \sin^2 (\beta_{LP}) \cos (2 \gamma_{LP} )]$$

and  $q_{zz}$  is the electric field gradient tensor,  $Q$  is the electric quadrupole moment, and  $\beta_{LP}$ ,  $\gamma_{LP}$  are the Euler angles defined from the principle axis of the electric field gradient tensor to the lab frame. The first term of the Hamiltonian is the zero order term representing the contribution of the static electric field,  $B_0$ , and determines the angular momentum energy levels,  $I_z$ . The second term is the first order correction that combines a spatial dependence ( $\omega_Q$ ), due to the interaction of the asymmetric nuclear charge distribution with the EFGs, and a spin-dependence ( $3 I_z^2 - I \cdot I$ ).

Another complication in this project arises from the fact that it uses solid-state NMR. As mentioned previously, magnetic resonance of liquids is a very useful tool in determining molecular structure because of its precision. Because of isotropic molecular tumbling, solution spectra have narrow and precise absorption peaks over reasonably small spectral widths. In our magnet the spectral width of a deuterated water molecule, for example, is 60 Hz. In a liquid spectrometer, this same spectral width would be even narrower with a value of less than 1 Hz. In contrast, the spectral width of a solid-state deuterated methyl group, in our magnet, is on the order of 50kHz. Another important feature of solid-state NMR spectra is that polycrystalline powders have broad powder spectra. This phenomenon can be partially understood by considering the rigidity of solids. In liquids molecules tumble freely, causing motional averaging that makes the NMR signal independent of the orientation of the molecule. However, a molecule locked into a crystal framework can not move in the same manner, and the orientation of the EFG and the magnetic field ( $\beta_{LP}$ ,  $\gamma_{LP}$ ) influence the NMR spectrum. This effect is particularly important when examining the number of distinct magnetic and chemical environments within a molecule. In many cases equivalent environments in liquids

become distinct in solids because they have different orientations with respect to the direction of the EFG tensor. Therefore, in solids there is an increase in the number of distinct orientations of the nuclei, with respect to  $B_0$  and the EFGs, that in turn gives rise to an increase in the number of different resonance frequencies of a molecule. These different resonance frequencies, however, only vary by small amounts, i.e. the resonance frequencies are very similar. The method of Fourier Transforming the FID signal cannot resolve this distribution of frequencies. Thus, they superimpose to produce a broad powder pattern lineshape. Nevertheless, although solid-state NMR cannot provide the molecular structure-fingerprint that liquid-NMR creates, by appropriate analysis, characteristics and behaviors of solids can be studied and quantified, from which an understanding of structure and dynamics can be obtained.

L-Cyclo (leucine-glycine)- $d_3$  is a cyclic dipeptide composed of two amino acids, leucine and glycine. Biologically, its significance derives from its potential to inhibit morphine addiction.[2] By examining this molecule in its solid state, we hope to elucidate the dynamics and to understand how they influence the binding of molecules in an organism's body. The extrapolation of this goal to the medical field would be to create a drug to be used to provide the same effect.

## IV. Experiment

All of the experiments for this project were conducted in the NMR Lab at The College of William and Mary. The basic NMR spectroscopy equipment used included a spectrometer operating at a deuteron Larmor frequency of 46.06 MHz, an Oxford 7-Tesla cryomagnet, a PTS-500 frequency synthesizer, a Wavetek 442 hi/lo filter, and an ENI LPI radiofrequency amplifier. The original free induction decay data was collected by the Libra Tecmag software and stored using the MacNMR 5.3 software. The files were later analyzed on an SGI unix workstation using modified PV-WAVE data visualization software.[2] The computer simulations were also conducted on an SGI unix workstation using EXPRESS, written by Robert Vold, Gina Hoatson, and Tak Tse at the College of William and Mary. [6] EXPRESS is used to simulate motion occurring in the fast, intermediate, and slow regimes, and can provide quadrupole echo lineshapes and partially relaxed spectra for both  $T_{1Z}$  and  $T_{1Q}$  relaxation processes.

### A. Temperature-Controlled Experiments

For each experiment the spectrometer was tuned for deuteron NMR using a deuterated water sample ( $D_2O$ ) in a static probe. After adjusting the spectrometer to ensure that the rf power and phases were well-defined, the L-cyclo (leucine-glycine)- $d_3$  sample was placed in the static probe. It was retuned and a quadrupolar echo sequence ( $90_x-\tau_1-90_y-\tau_2$ ) was used to collect the spectra. Typical parameters were:  $90^\circ$  pulses 1.6  $\mu s$  long, with a  $\tau_1=50 \mu s$  delay between the pulses, and a  $\tau_2=32.8 \mu s$  delay between the second pulse and the data acquisition. The spectral width was 52.083 kHz, and the

recycle time,  $\tau_r$ , ranged from 400ms to 700ms, depending on the temperature-dependent relaxation time,  $T_{1Z}$ .

All of the experiments were temperature-controlled by flowing nitrogen or compressed air through the probe. The range of temperatures investigated was between 100°C and -72°C. The equipment used to attain a specific temperature included a preheater and Lakeshore temperature controller connected to a non-inductively-wound resistance heater, with a temperature sensor located close to the sample coil of the probe. For the low temperature experiments, nitrogen was passed through a dewar filled with liquid nitrogen, and then flowed over the heater assembly. Once the desired temperature was achieved, as measured on the Lakeshore Platinum resistance sensor, the probe was allowed to equilibrate for twenty minutes. Then, before data collection was begun, the probe was retuned to be resistive at 46.06 MHz; 50 $\Omega$  and less than +/- 1° phase on the network analyzer.

The L-cyclo (leucine-glycine)-d<sub>3</sub> used was the same sample Olsen used in his experiments. It was synthesized in 1996 by Professor Deborah Bebout and her students in Chemistry Department at the College of William and Mary.[2] During the experiments, some problems were encountered, because after sustained periods at high temperature, the sample would absorb water. To alleviate this problem the sample was dried in Professor Bebout's laboratory and stored over a desiccant while not used in the experiments.

The observed temperature-dependent deuteron quadrupolar echo spectra are presented, for the high temperature range, 10°C to 100°C, and for the low temperature range, -72°C to -10°C, in Figures 4 and 5, respectively.

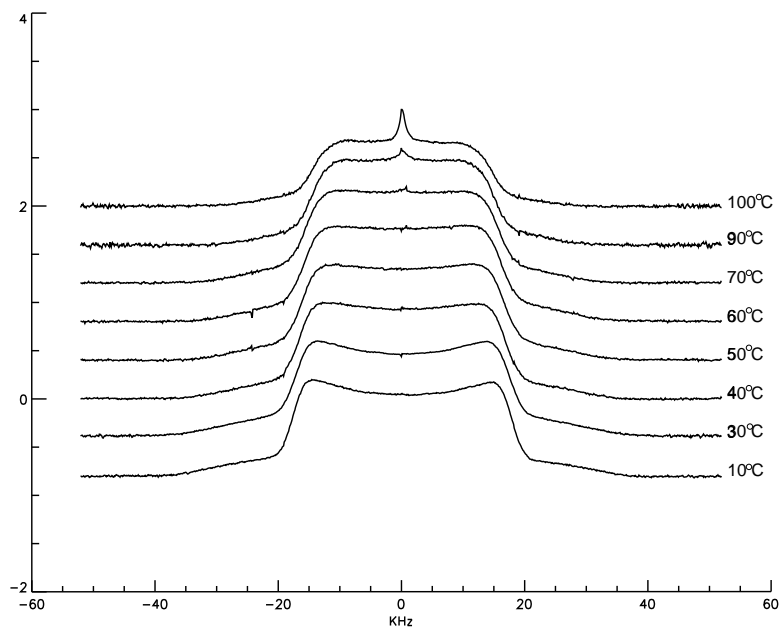


Figure 4: Deuteron Quadrupolar Echo Spectra for Experiments Between +10°C and +100°C, with the experiment temperature noted (in °C) to the right of each lineshape. The spectra were plotted with a difference of y offset for clarity.

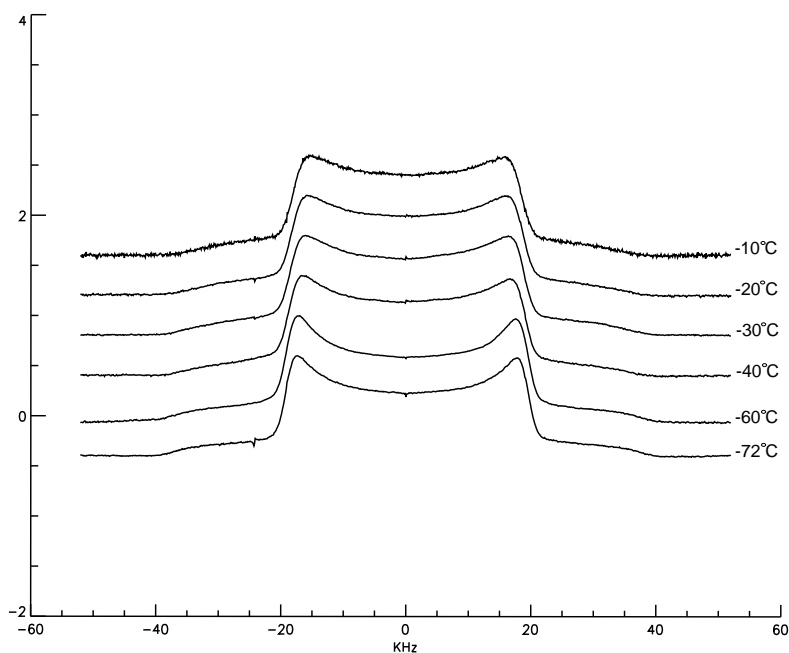


Figure 5: Deuteron Quadrupolar Echo Spectra for Experiments Between -72°C and -10°C, with the experiment temperature noted (in °C) to the right of each lineshape. The spectra were plotted with a difference of y offset for clarity.

## B. Computer Simulations

The additional motion seen in the L-cyclo (leucine-glycine)-d<sub>3</sub> was hypothesized to be in the intermediate regime, and EXPRESS was used to simulate the observed dynamics. To run a simulation, a model of the anticipated motion must be created and the appropriate parameter values chosen. In the EXPRESS input file, the user can create multiple frames of motion, prescribing the particular motion in each frame. To simulate the observed experimental motion, we used three different models. In each model there was one frame of motion, but the number of jump sites varied from four to six to twenty. For each of the jump sites, the corresponding Euler angles ( $\alpha$ ,  $\beta$ ,  $\gamma$ ) were specified. We assumed that each jump site was equally populated, i.e. equi-probable, and that each site was able to "jump" to any of the other sites without restrictions of connectivity or proximity. In addition, certain parameters, corresponding to experimental conditions, such as the pulse widths, the pulse spacing, the spectral width, the number of points in the FID, and the Larmor frequency, were given to the input file. For each model the two main parameters to be determined were the quadrupole coupling constant (QCC) and the rate of motion.

As discussed in Olsen's original work on L-Cyclo (leucine-glycine)-d<sub>3</sub>, there exists fast three-site rotation of the deuterated methyl group. We accounted for this motion in our simulated models using a motionally averaged quadrupole coupling constant. The QCC value for a static methyl group is approximately 169 kHz. Fast three-site methyl rotation reduces this QCC value by a factor of one-third. [7] Therefore, we used a quadrupole coupling value of QCC = 56 kHz for all of the simulations.

One challenging aspect of creating the simulation models was determining the corresponding Euler angles. For the four and six site models, this analysis was relatively straightforward. The twenty site model, however, proved more challenging. For EXPRESS, the Euler angles are defined as  $\alpha$ ,  $\beta$ ,  $\gamma$ . In our models  $\gamma$  is zero because we assume a cylindrically symmetric EFG tensor. Then,  $\alpha$  and  $\beta$  correspond to the polar angles  $\phi$  and  $\theta$ , respectively, where  $\phi$  is the rotation about the z-axis and  $\theta$  is the angle measured down from the positive z-axis, as shown in Figure 6.

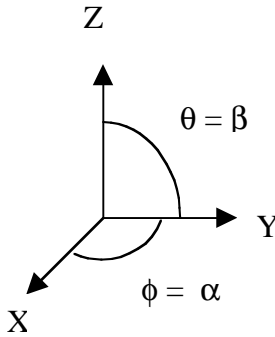


Figure 6: Illustration of Euler angles.

### 1. Four Site Model

The four site simulation model was based on the geometry of a tetrahedron, with possible jumps sites at its vertices, for which the angles are listed in Table 1.

Table 1: Euler Angles in Degrees for the Four Site Model

$\alpha$	$\beta$	$\gamma$
0	0	0
0	109.4712	0
120	109.4712	0
240	109.4712	0

The simulated quadrupolar echo spectra for this model are presented in Figures 7 and 8, with rates of motion between  $1 \times 2 \text{ s}^{-1}$  and  $9 \times 3 \text{ s}^{-1}$ .

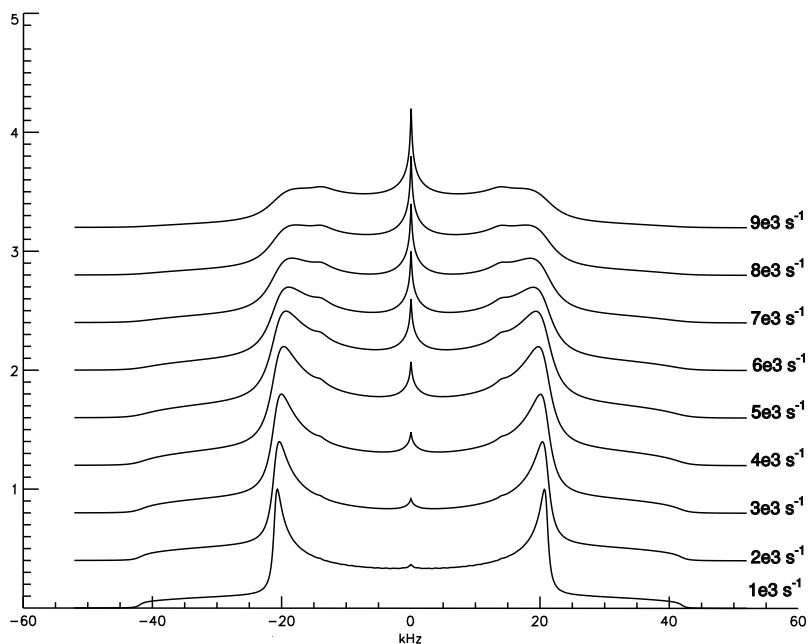


Figure 7: Simulated Quadrupolar Echo Spectra for the Four Site Jump Model with Rates of Motion Between  $1 \times 3 \text{ s}^{-1}$  and  $9 \times 3 \text{ s}^{-1}$ , with the simulated rate noted (in  $\text{s}^{-1}$ ) to the right of each lineshape. The spectra were plotted with a difference of y offset for clarity.

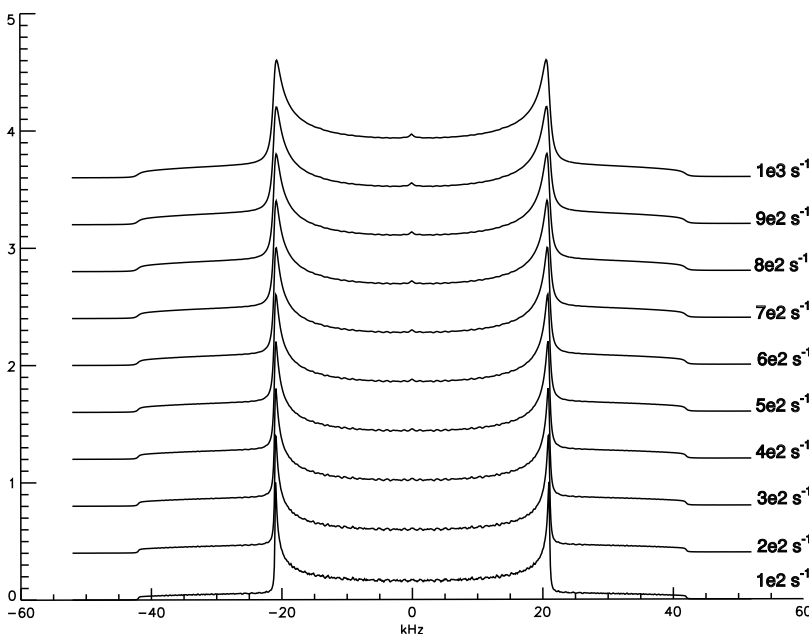


Figure8: Simulated Quadrupolar Echo Spectra for the Four Site Jump Model with Rates of Motion Between  $1 \times 2 \text{ s}^{-1}$  and  $1 \times 3 \text{ s}^{-1}$ , with the simulated rate noted (in  $\text{s}^{-1}$ ) to the right of each lineshape. The spectra were plotted with a difference of y offset for clarity.

## 2. Six Site Model

The six site model used the vertices of an octahedron as its possible jump sites. There were two sites in the z direction, one on the positive z-axis and the other along the negative z-axis. The other four sites were at equally spaced angles in the X-Y plane. The corresponding numerical values for the angles are listed in Table 2.

*Table 2: Euler Angles in Degrees for the Six Site Model*

$\alpha$	$\beta$	$\gamma$
0	0	0
0	180	0
0	90	0
90	90	0
180	90	0
270	90	0

The simulated quadrupolar echo spectra for this model are presented in Figures 9 and 10, with rates of motion between  $1 \times 10^2 \text{ s}^{-1}$  and  $9 \times 10^3 \text{ s}^{-1}$ .

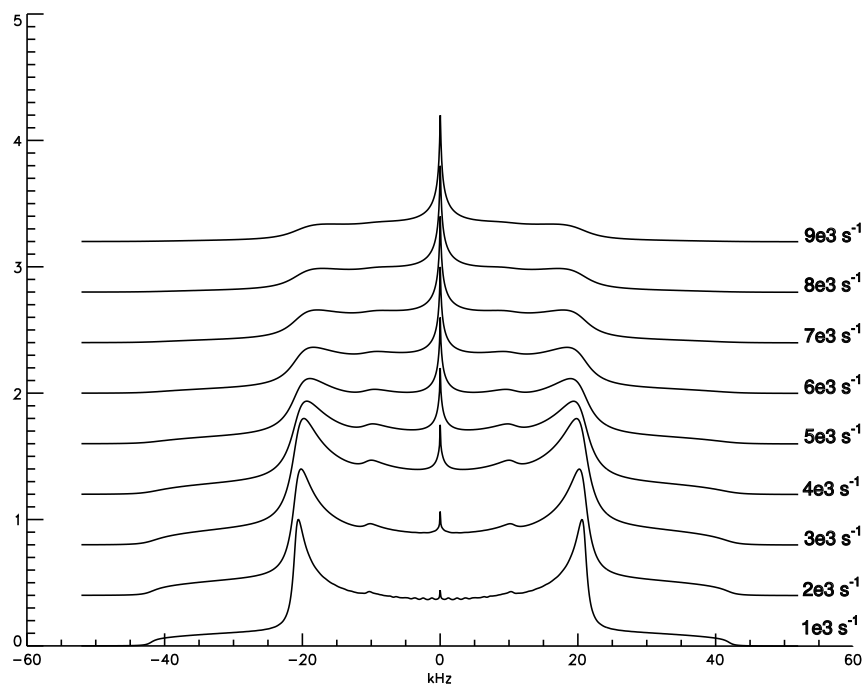


Figure 9: Simulated Quadrupolar Echo Spectra for the Six Site Jump Model with Rates of Motion Between  $1 \times 3 \text{ s}^{-1}$  and  $9 \times 3 \text{ s}^{-1}$ , with the simulated rate noted (in  $\text{s}^{-1}$ ) to the right of each lineshape. The spectra were plotted with a difference of y offset for clarity.

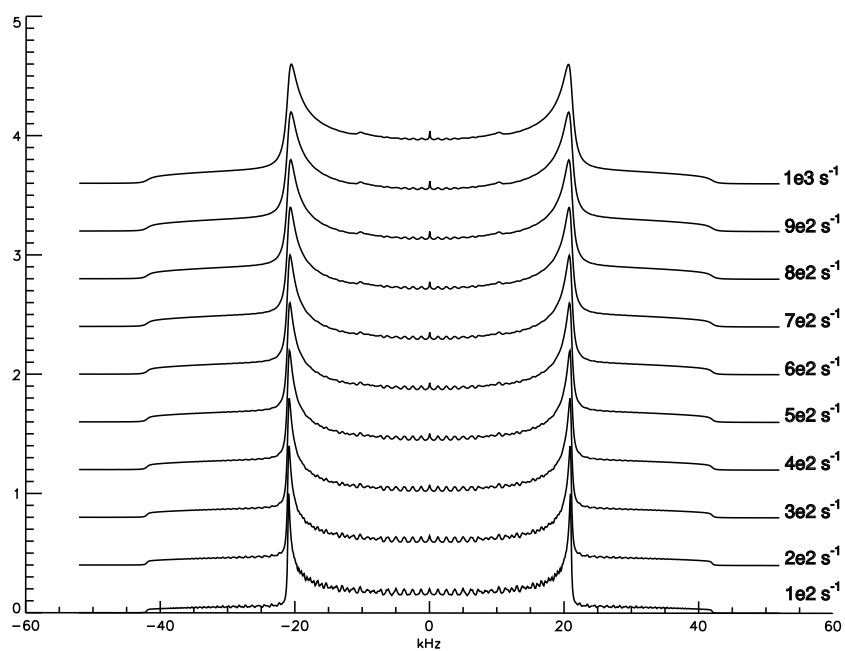
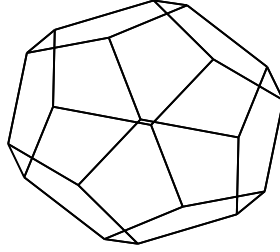


Figure 10: Simulated Quadrupolar Echo Spectra for the Six Site Jump Model with Rates of Motion Between  $1 \times 2 \text{ s}^{-1}$  and  $1 \times 3 \text{ s}^{-1}$ , with the simulated rate noted (in  $\text{s}^{-1}$ ) to the right of each lineshape. The spectra were plotted with a difference of y offset for clarity.

### 3. Twenty Site Model

For the twenty site simulation, the vertices of a regular dodecahedron were used as the jump sites. The process for determining the Euler angles was complex. First, the polygon was plotted using the Maple computer program, as seen in Figure 11.



*Figure 11: Illustration of a Regular Dodecahedron*

Then, this program was used to find the vertices of a regular dodecahedron inscribed in a circle of radius one. Since we were only concerned with the angular position of the vertices, the length of the radius was arbitrary. After obtaining coordinates for all twenty vertices in the  $x, y, z$  coordinate system, it took a good deal of work to determine  $\alpha$  and  $\beta$  for each vertex. Using the knowledge that, in our models,  $\alpha$  and  $\beta$  are equivalent to the polar angles  $\phi$  and  $\theta$ , the following relationships were determined:

$$\alpha = (1/2) \arccos ((x^2 - y^2)/(1 - z^2))$$

$$\beta = \arccos (z)$$

The second equation gave the correct value of  $\beta$  directly, while, for the first equation, it was necessary to consider in which quadrant the vertex was to determine the correct value of  $\alpha$ . The values of the Euler angles for a regular dodecahedron are listed in Table 3.

*Table 3: Euler Angles in Degrees for the Twenty Site Model*

$\alpha$	$\beta$	$\gamma$
290.905	90	0
249.095	90	0
240	54.736	0
270	20.905	0
300	54.736	0
90	159.095	0
120	125.264	0
110.905	90	0
69.095	90	0
60	125.264	0

$\alpha$	$\beta$	$\gamma$
270	159.095	0
240	125.264	0
180	110.905	0
180	69.095	0
120	54.736	0
90	20.905	0
60	54.736	0
0	69.095	0
0	110.905	0
300	125.264	0

The simulated quadrupolar echo spectra for this model are presented in Figures 11 and 12, with rates of motion between  $1 \times 2 \text{ s}^{-1}$  and  $9 \times 3 \text{ s}^{-1}$ .

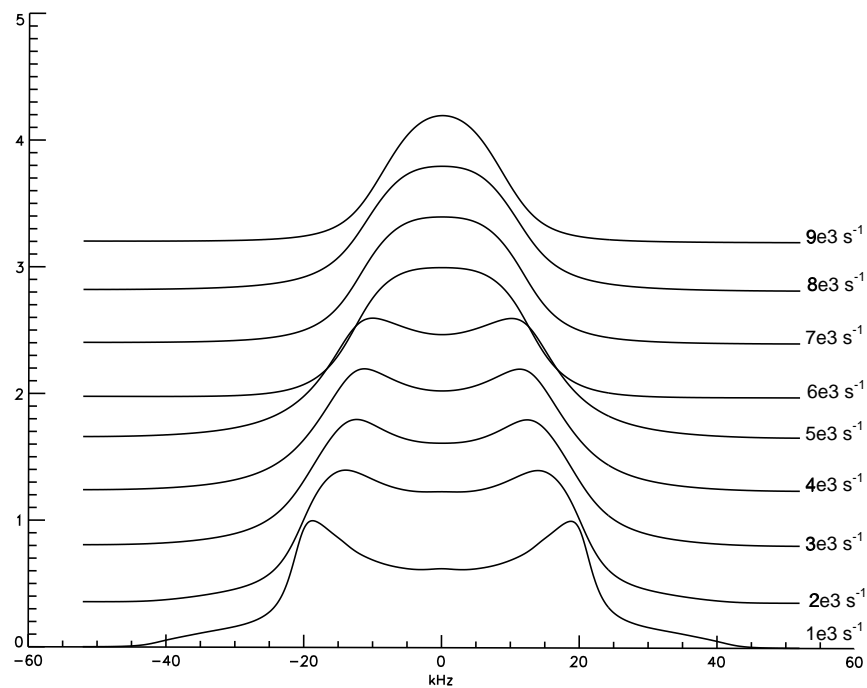


Figure 11: Simulated Quadrupolar Echo Spectra for the Twenty Site Jump Model with Rates of Motion Between  $1 \times 3 \text{ s}^{-1}$  and  $9 \times 3 \text{ s}^{-1}$ , with the simulated rate noted (in  $\text{s}^{-1}$ ) to the right of each lineshape. The spectra were plotted with a difference of y offset for clarity.

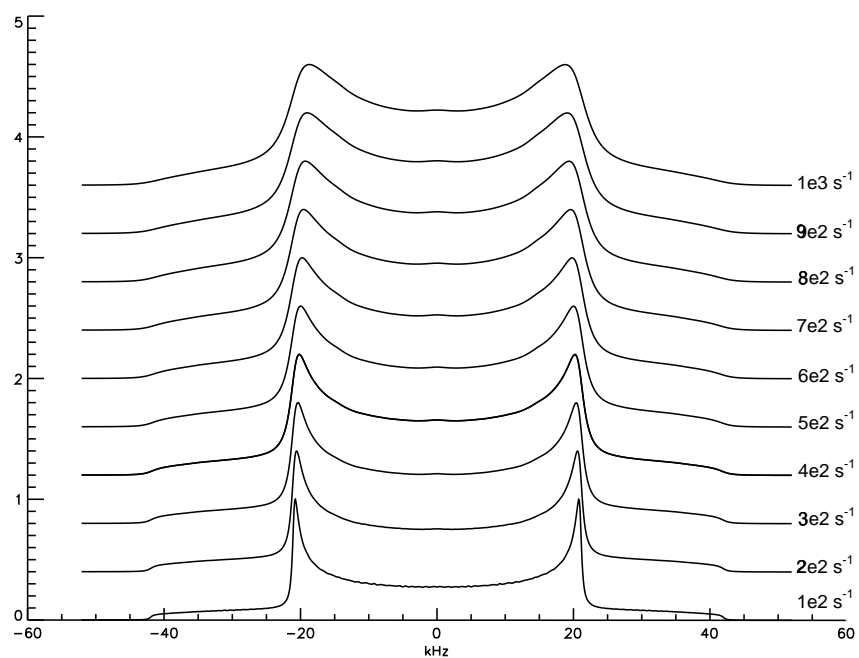


Figure 12: Simulated Quadrupolar Echo Spectra for the Twenty Site Jump Model with Rates of Motion Between  $1 \times 2 \text{ s}^{-1}$  and  $1 \times 3 \text{ s}^{-1}$ , with the simulated rate noted (in  $\text{s}^{-1}$ ) to the right of each lineshape. The spectra were plotted with a difference of y offset for clarity.

## V. Results and Discussion

### A. Temperature-Controlled Experiments

The first goal of this project was to determine if, in fact, there was some type of supplemental motion occurring in L-cyclo (leucine-glycine)-d<sub>3</sub>, in addition to the fast three-site rotation of the methyl group. The results of the temperature-controlled experiments support the existence of this composite motion. As discussed previously, the fast dynamics of the methyl group motionally averages the quadrupole coupling constant of the static methyl group by a factor of one third. If no additional motion existed, then the quadrupolar echo lineshapes and the motionally averaged QCC value should have remained constant regardless of the temperature. (The methyl rotation is in the fast limit, so it does not affect the lineshape, other than by reducing the QCC to a lower, but still constant, value.) The experimental spectra, however, do change with temperature. At a temperature close to room temperature, 30°C, the observed spectrum resembled the expected broadened powder pattern with a quadrupole coupling constant averaged over the fast methyl rotation. It was table-like with a slight central dip. As the temperature was decreased, the intensity of the center of the powder pattern decreased and the shoulders of the powder pattern broadened. [See Figure 4] These changes in the lineshape corresponded to the anticipated decrease in thermally-activated molecular motion at lower temperatures. Since these patterns remained as the temperature was lowered, the spectra prove that the second type of molecular motion was being frozen out. Thus, at low temperatures the molecule dynamics were slowed down.

In contrast, as the temperature was increased, the powder pattern width became slightly narrower and the central region of the powder pattern rose to become flatter. Then, at temperatures of 90°C and 100°C, a central spike appeared, a possible indicator of fast molecular motion. [See Figure 5] These changes in the lineshape in the high temperature limit demonstrate that the hypothesized additional motion is occurring. (Because of the temperature limitations of the equipment, currently, experiments above 100°C are not possible.)

The values of the motionally averaged quadrupole coupling constant ( $\langle QCC \rangle$ ) for the experiments are presented in Table 4 and Figure 13. At the elevated temperatures, motional averaging is increased which initiates collapse of the powder pattern and the corresponding decrease in the  $\langle QCC \rangle$  value.

*Table 4: Experimental Temperature-Dependent Quadrupole Coupling Constant Values*

T (°C)	Error (°C)	$\langle QCC \rangle$ (kHz)	Error (kHz)
-72.0	+/- 0.5	53.5	+/- 0.2
-60.0	+/- 0.5	51.9	+/- 0.2
-40.0	+/- 0.5	50.1	+/- 0.2
-30.0	+/- 0.5	48.2	+/- 0.2
-20.0	+/- 0.5	48.2	+/- 0.2
-10.0	+/- 0.5	46.4	+/- 0.2
+10.0	+/- 0.5	45.2	+/- 0.2
+30.0	+/- 0.5	42.0	+/- 0.2
+40.0	+/- 0.5	42.9	+/- 0.2
+50.0	+/- 0.5	40.2	+/- 0.2
+60.0	+/- 0.5	39.6	+/- 0.2
+70.0	+/- 0.5	37.1	+/- 0.4
+80.0	+/- 0.5	36.3	+/- 0.4
+90.0	+/- 0.5	35.9	+/- 0.4
+100.0	+/- 0.5	36.2	+/- 0.4

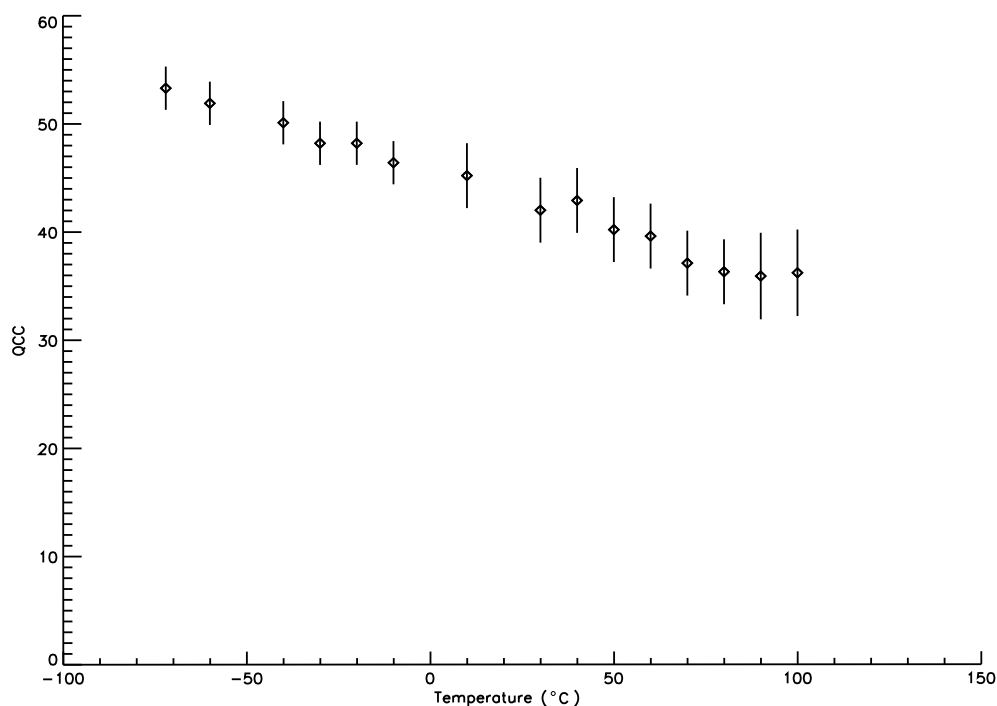


*Figure 13: Changes in Quadrupole Coupling Constant Value with Temperature*

The problem of water contaminating the sample, noted in the previous section, did affect some of the results. The contamination was identified when the intensity of the central peak for the 100°C scan appeared to be of a lower intensity than that of the previous 90°C experiment. If the central peak was caused by molecular motion, then a higher temperature should increase the rate of dynamics, thereby generating a central peak of higher intensity at 100°C than at 90°C. To verify the origin of the observed spike, the sample was dried, and the experiment run again at 90°C. The second 90°C experiment still produced a central spike, but with an intensity much less than that of the first run. At first, it was hypothesized that molecular motion was the primary cause of the central spike, while absorption of water into the sample only increased the intensity of the peak. Yet, this hypothesis is not well-grounded. Therefore, the appearance of the central

spike should be taken into consideration when analyzing the experiment, but proof, understanding, and explanation of this additional molecular motion should not be based strongly on this central peak, since there is not enough evidence to prove that it is not just an aberration.

## B. Computer Simulations

The three main distinctive characteristics of the experimental data were the flat, broad, table-like spectra, the decreasing quadrupole coupling constant with increasing temperature, and the appearance of a central spike at high temperatures (although we are not sure of its origin, it is a characteristic of the experimental data). Starting with a simple model, the four site model, we attempted to find the same three characteristics in simulated spectra. While the four and six site models both produced spectra that started with a central dip at low rates of motion that progressed to a sharp peak at higher rates, (where an increased rate corresponds to an increase in temperature, since we are considering thermally-activated motion), neither model successfully captured the changes seen in the quadrupole coupling constant. Therefore, a more complex model was selected: the twenty site simulation.

The twenty site model did achieve the sought after change by reducing the powder pattern splitting as the rate of motion increased. However, a new caveat was introduced by the complex model: it did not produce a sharp peak. After carefully examining all three models with rates of motion between  $1 \times 10^2 \text{ s}^{-1}$  and  $9 \times 10^3 \text{ s}^{-1}$ , it seemed that the twenty-site model best fit the experimental results, despite its lack of a sharp central spike. Both the four and six site models produced jagged spectra. In addition to having the central spike, the shoulders of their powder lineshapes were also

narrower and steeper than the experimental spectra. The twenty site model produced lineshapes that approached a solitary peak by more rounded and softer changes.

The following pages provide tables and plots of the powder pattern splitting for the three different models. In the experimental results a decrease in the thermally averaged quadrupole coupling constant was seen. The powder pattern splitting is proportional to the thermally averaged quadrupole coupling constant. Therefore, a decrease in the powder pattern splitting should also be seen. For the four and six site models (Figures 14 and 15, respectively), while there is a small decrease in the powder pattern splitting, it is not as dramatic as it is in the twenty-site simulation (Figure 16).

Thus, by looking at the general characteristics of the simulation results, two important ideas emerge. First, the simulated spectra provide support for the hypothesis that the central spike in the experimental results is due to absorption of water into the sample. Second, the twenty-site jump model appears to be the best representation of the observed molecular motion, given the three different models tested.

Table 5: Simulated Rate-Dependent Powder Pattern Splitting Values for the Four Site Jump Model

Rate (s <sup>-1</sup> )	Splitting (kHz)	Error (kHz)
1 x 10 <sup>2</sup>	41.9	+/- 0.1
2 x 10 <sup>2</sup>	41.9	+/- 0.1
3 x 10 <sup>2</sup>	41.7	+/- 0.1
4 x 10 <sup>2</sup>	41.7	+/- 0.1
5 x 10 <sup>2</sup>	41.7	+/- 0.1
6 x 10 <sup>2</sup>	41.7	+/- 0.1
7 x 10 <sup>2</sup>	41.5	+/- 0.1
8 x 10 <sup>2</sup>	41.5	+/- 0.1
9 x 10 <sup>2</sup>	41.5	+/- 0.1

Rate (s <sup>-1</sup> )	Splitting (kHz)	Error (kHz)
1 x 10 <sup>3</sup>	41.5	+/- 0.1
2 x 10 <sup>3</sup>	40.9	+/- 0.2
3 x 10 <sup>3</sup>	40.4	+/- 0.2
4 x 10 <sup>3</sup>	39.9	+/- 0.2
5 x 10 <sup>3</sup>	39.1	+/- 0.2
6 x 10 <sup>3</sup>	38.2	+/- 0.4
7 x 10 <sup>3</sup>	37.6	+/- 0.4
8 x 10 <sup>3</sup>	37.2	+/- 0.4
9 x 10 <sup>3</sup>	34.6	+/- 0.4

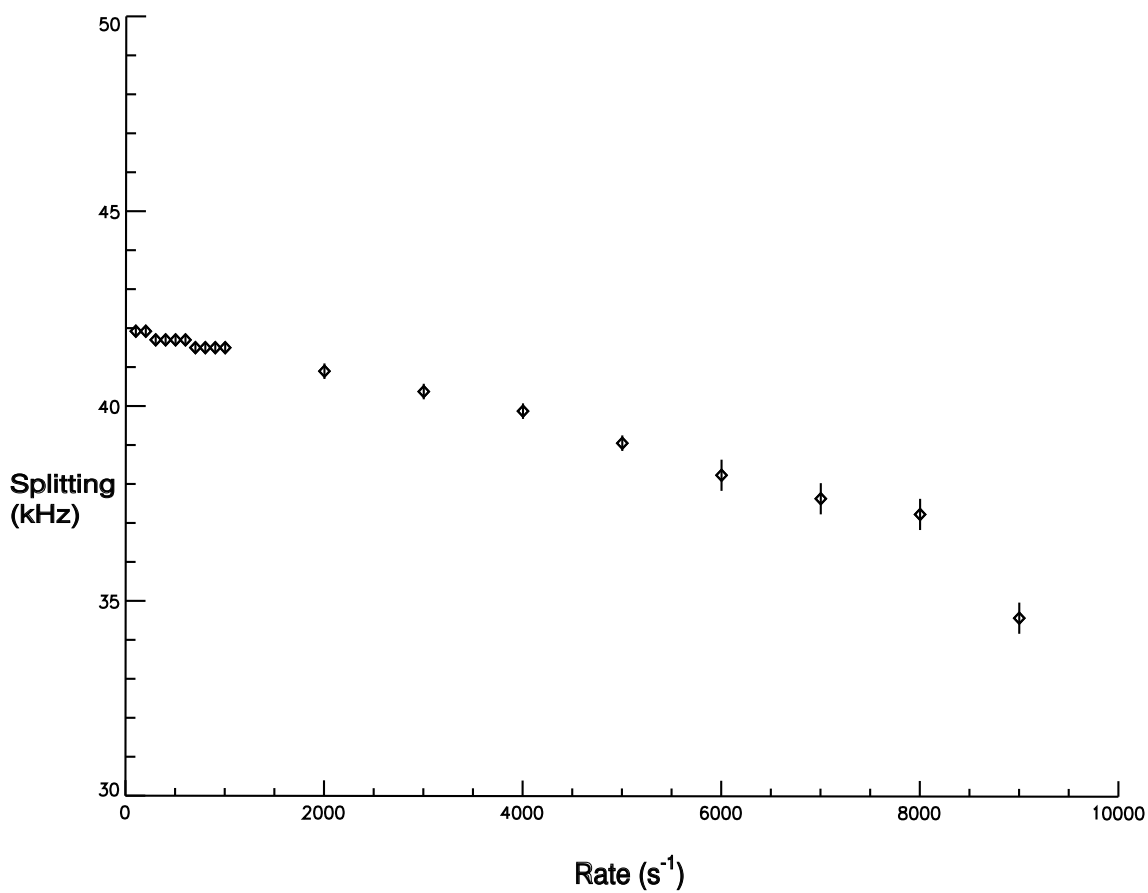


Figure 14: Changes in Powder Pattern Splitting Value with Rate for the Four Site Jump Model

Table 6: Simulated Rate-Dependent Powder Pattern Splitting Values for Six Site Jump Model

Rate (s <sup>-1</sup> )	Splitting (kHz)	Error (kHz)
1 x 10 <sup>2</sup>	41.9	+/- 0.1
2 x 10 <sup>2</sup>	41.9	+/- 0.1
3 x 10 <sup>2</sup>	41.7	+/- 0.1
4 x 10 <sup>2</sup>	41.7	+/- 0.1
5 x 10 <sup>2</sup>	41.7	+/- 0.1
6 x 10 <sup>2</sup>	41.7	+/- 0.1
7 x 10 <sup>2</sup>	41.5	+/- 0.1
8 x 10 <sup>2</sup>	41.5	+/- 0.1
9 x 10 <sup>2</sup>	41.5	+/- 0.1

Rate (s <sup>-1</sup> )	Splitting (kHz)	Error (kHz)
1 x 10 <sup>3</sup>	41.3	+/- 0.1
2 x 10 <sup>3</sup>	40.7	+/- 0.2
3 x 10 <sup>3</sup>	40.3	+/- 0.2
4 x 10 <sup>3</sup>	39.9	+/- 0.2
5 x 10 <sup>3</sup>	39.1	+/- 0.2
6 x 10 <sup>3</sup>	37.0	+/- 0.4
7 x 10 <sup>3</sup>	35.9	+/- 0.4
8 x 10 <sup>3</sup>	34.5	+/- 0.4
9 x 10 <sup>3</sup>	33.0	+/- 0.4

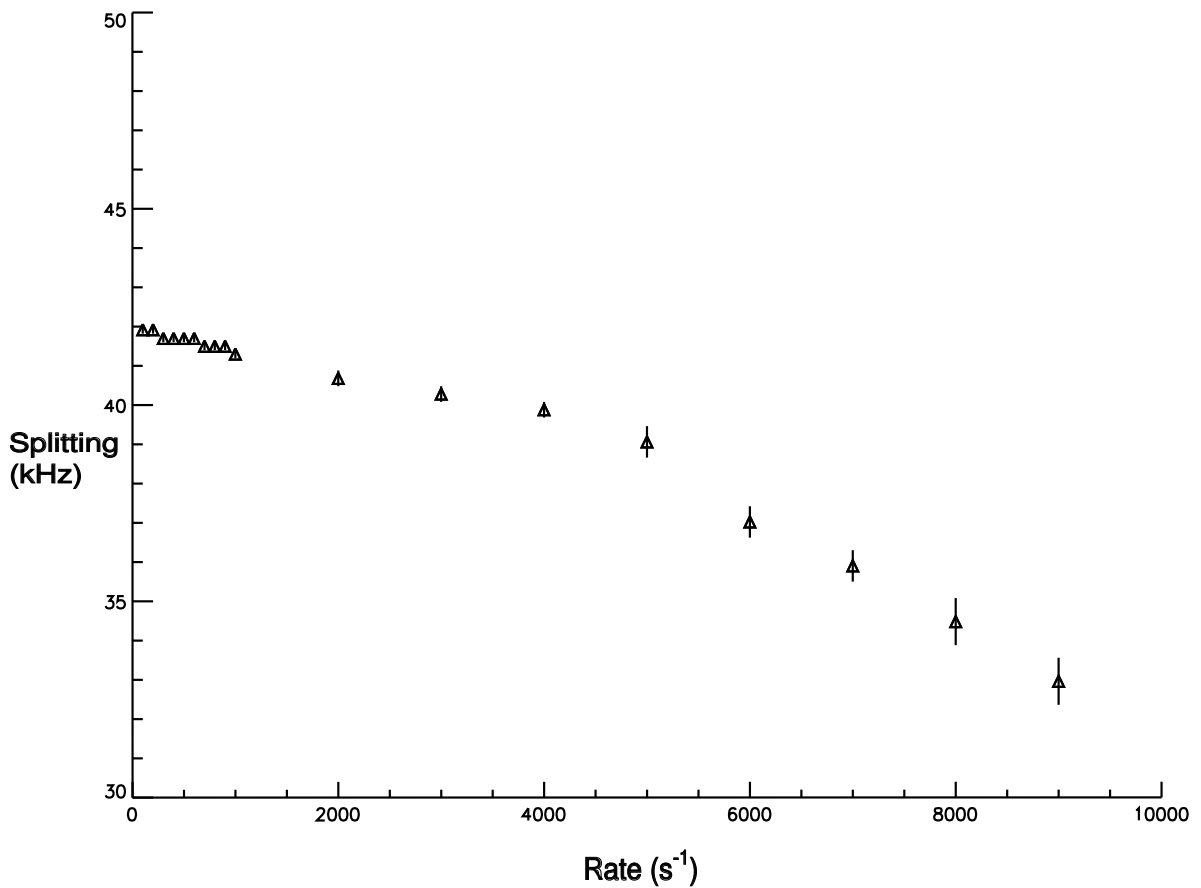


Figure 15: Changes in Powder Pattern Splitting Value with Rate for the Six Site Jump Model

Table 7: Simulated Rate-Dependent Powder Pattern Splitting Values for Twenty Site Jump Model

Rate (s <sup>-1</sup> )	Splitting (kHz)	Error (kHz)
1 x 10 <sup>2</sup>	41.7	+/- 0.1
2 x 10 <sup>2</sup>	41.3	+/- 0.1
3 x 10 <sup>2</sup>	40.9	+/- 0.1
4 x 10 <sup>2</sup>	40.5	+/- 0.1
5 x 10 <sup>2</sup>	40.1	+/- 0.2
6 x 10 <sup>2</sup>	39.7	+/- 0.2
7 x 10 <sup>2</sup>	39.3	+/- 0.2
8 x 10 <sup>2</sup>	38.7	+/- 0.2
9 x 10 <sup>2</sup>	38.2	+/- 0.2

Rate (s <sup>-1</sup> )	Splitting (kHz)	Error (kHz)
1 x 10 <sup>3</sup>	37.6	+/- 0.2
2 x 10 <sup>3</sup>	28.1	+/- 0.4
3 x 10 <sup>3</sup>	24.8	+/- 0.4
4 x 10 <sup>3</sup>	22.6	+/- 0.4
5 x 10 <sup>3</sup>	20.1	+/- 0.4
6 x 10 <sup>3</sup>	26.0	+/- 0.2
7 x 10 <sup>3</sup>	24.5	+/- 0.2
8 x 10 <sup>3</sup>	22.4	+/- 0.2
9 x 10 <sup>3</sup>	18.7	+/- 0.2

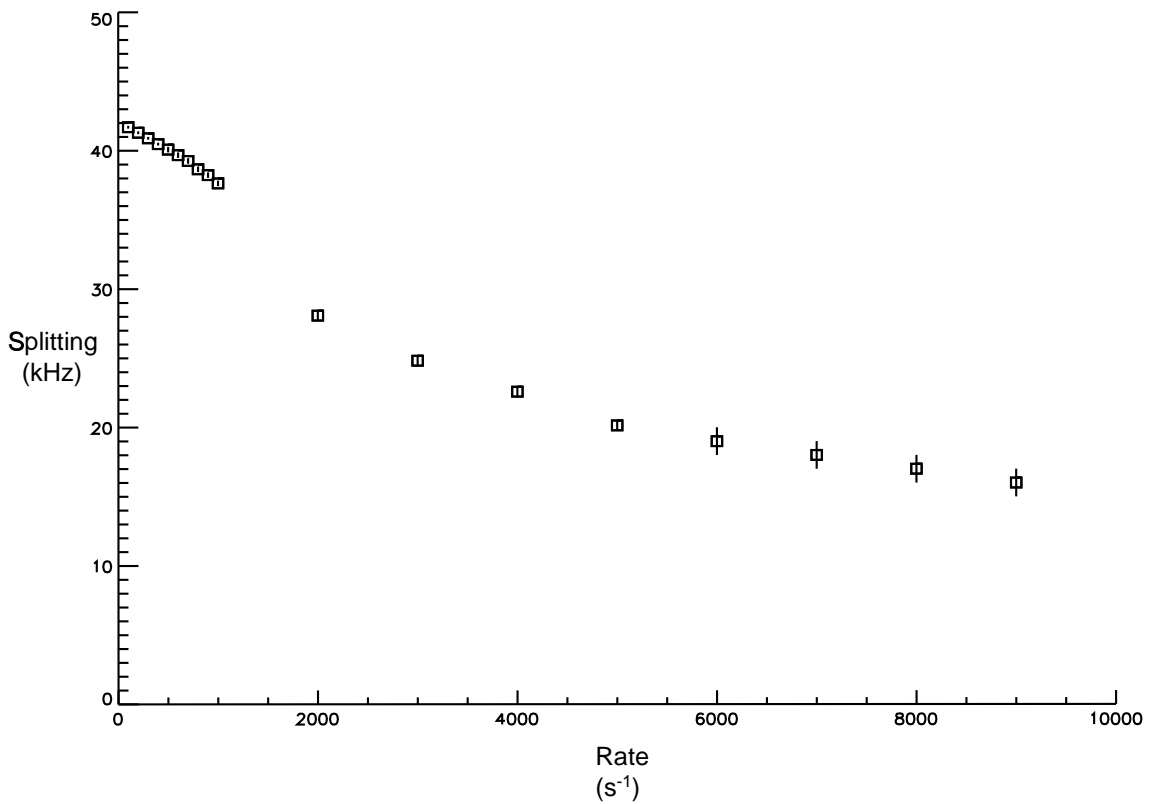


Figure 16: Changes in Powder Pattern Splitting Value with Rate for the Twenty Site Jump Model

### C. Comparison of Simulations to Experimental Data

After considering the general traits and patterns of the spectra for the different models, a closer comparison of a few spectra is needed. For this comparison, one low temperature, negative 60°C, and one high temperature, 100°C, were selected. Then, for each model, it was necessary to pick the rate whose lineshape best matched the experimental spectrum for the given temperature. After some initial comparisons, it appeared that our quadrupole coupling constant was too large, meaning that the shoulders of the powder pattern were too wide. After the value for the rate was narrowed down to a smaller range, those few rates were rerun through EXPRESS, but this time with lower QCC values. Since the selection of a quadrupole coupling constant of  $QCC = 56\text{kHz}$  was based on loose parameters, it was legitimate to vary the QCC-value slightly to obtain a better fit. (The QCC of a static methyl group is approximately 169kHz. However, the experimental range of the motionally averaged QCC for fast three site methyl rotation is between 45 – 55 kHz. [7])

Comparisons of the negative 60°C spectrum with a 4-site, 6-site, and 20-site simulation are presented in Figures 17, 18, and 19, respectively. For this temperature the four site model matched the experimental results with a rate of  $4 \times 10^3 \text{ s}^{-1}$ , the six site model with a rate of  $3 \times 10^3 \text{ s}^{-1}$ , and the twenty site model with a rate of  $9 \times 10^2 \text{ s}^{-1}$ .

Comparisons of the highest temperature spectrum, 100°C, with a 4-site, 6-site, and 20-site simulation are illustrated in Figures 20, 21, 22, respectively. For this temperature the four site model matched the experimental results with a rate of  $1 \times 10^4 \text{ s}^{-1}$ , the six site model with a rate of  $1 \times 10^4 \text{ s}^{-1}$ , and the twenty site model with a rate of  $4 \times 10^3 \text{ s}^{-1}$ .

Therefore, by comparing the simulated and experimental results more closely, the hypothesis from the previous section still holds true: the twenty-site jump model produced the best representation of the experimental spectra.

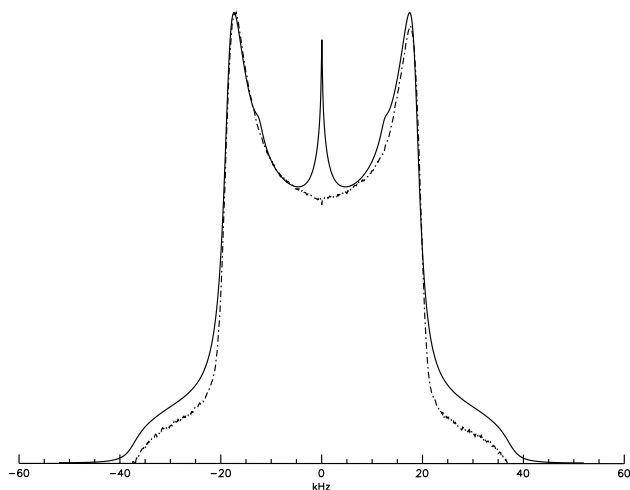


Figure 17: Comparison of  $-60^{\circ}\text{C}$  Quadrupolar Echo Spectrum (dashed line) to Four Site Model Spectrum at a rate of  $4 \times 10^3 \text{ s}^{-1}$  (solid line) and a  $QCC = 50 \text{ kHz}$ .

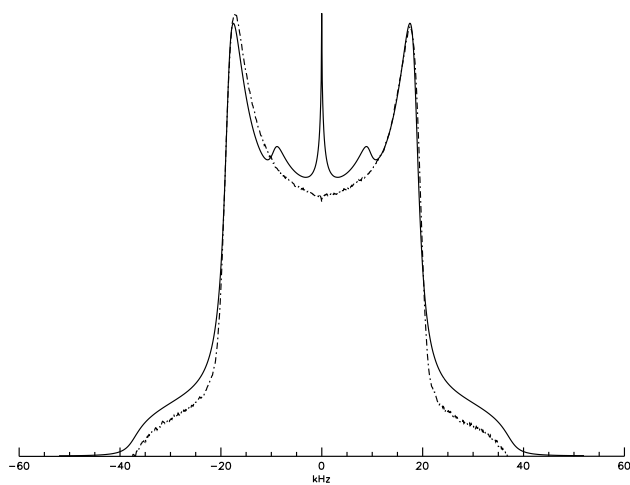


Figure 18: Comparison of  $-60^{\circ}\text{C}$  Quadrupolar Echo Spectrum (dashed line) to Six Site Model Spectrum at a rate of  $3 \times 10^3 \text{ s}^{-1}$  (solid line) and a  $QCC = 50 \text{ kHz}$ .

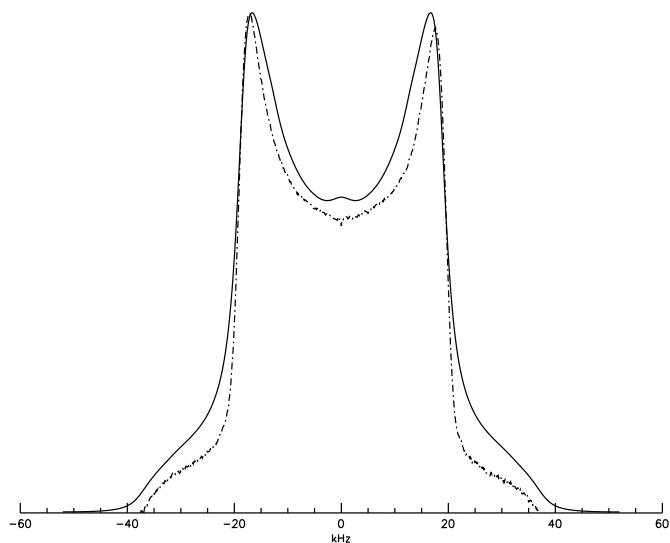


Figure 19: Comparison of  $-60^{\circ}\text{C}$  Quadrupolar Echo Spectrum (dashed line) to Twenty Site Model Spectrum at a rate of  $9 \times 10^2 \text{ s}^{-1}$  (solid line) and a  $QCC = 50 \text{ kHz}$ .

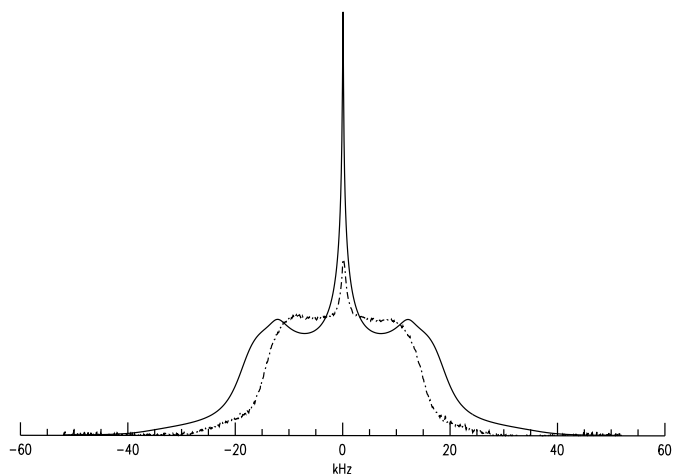


Figure 20: Comparison of 100°C Quadrupolar Echo Spectrum (dashed line) to Four Site Model Spectrum at a rate of  $1 \times 10^4 \text{ s}^{-1}$  (solid line) and a QCC = 50 kHz.

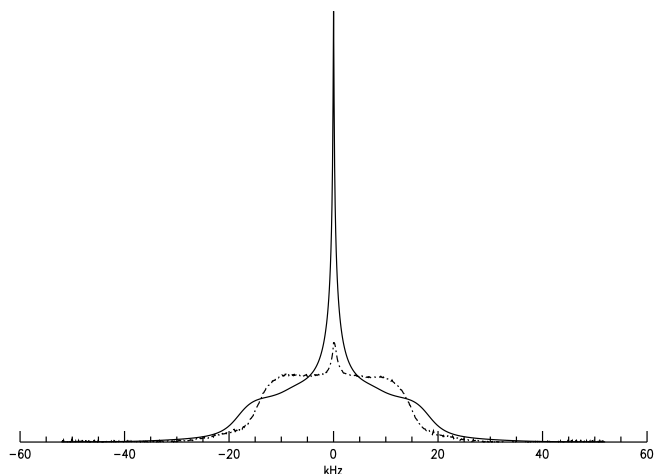


Figure 21: Comparison of 100°C Quadrupolar Echo Spectrum (dashed line) to Six Site Model Spectrum at a rate of  $1 \times 10^4 \text{ s}^{-1}$  (solid line) and a QCC = 50 kHz.

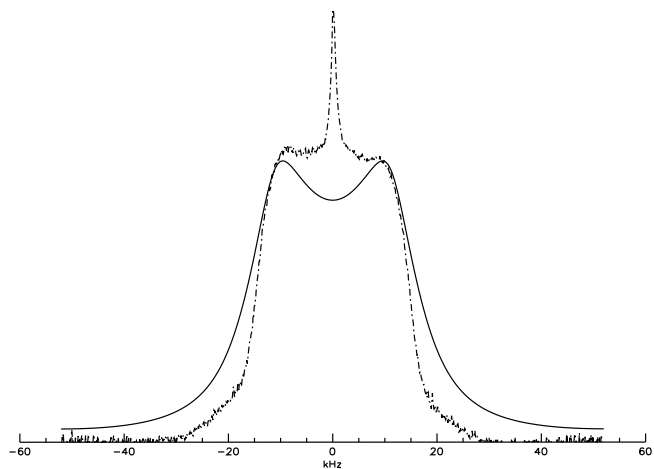


Figure 22: Comparison of 100°C Quadrupolar Echo Spectrum (dashed line) to Twenty Site Model Spectrum at a rate of  $4 \times 10^3 \text{ s}^{-1}$  (solid line) and a QCC = 50 kHz.

## VII. Conclusions

The quadrupole echo spectra of L-cyclo(leucine-glycine)-d<sub>3</sub> exhibit unusual characteristics, mainly the change in the powder lineshape, the appearance of a central spike at high temperatures, and the change in the observed quadrupole coupling constant. These experimental spectral deviations support the results of Olsen's previous research that concluded that there exists additional molecular motion in L-cyclo (leucine-glycine)-d<sub>3</sub>, beyond the anticipated three-site methyl rotation. However, there is some ambiguity because the absorption of water distorted a few of the experimental results, and it is not possible to determine, without further high temperature experiments, the characteristics of the central region of L-cyclo(leucine-glycine)-d<sub>3</sub> spectra.

Assuming that the central spike that appeared in the experimental spectra was just absorbed water, the twenty-site jump model best fits the other characteristics of the experimental data: it exhibits the broad table-like powder lineshape and its splitting decreases with increasing thermal activity. The simulated twenty site model gradually advances towards a single peak at higher rates, and the change to a single peak is not as sharp and jagged as the four or six site model. The experimental data supports this softer approach to one peak. Furthermore, because an increase in the number of jump sites improved the correlation of the experimental data to simulated results, the additional motion in is probably diffusive, since diffusive motion would be a continuum of an infinite number of jump sites. However, further experimentation and more simulations are needed to determine the activation parameters of this thermally-activated process to prove it the dynamics are diffusive jumps.

An initial estimate of the activation parameters can be obtained by evaluating the two simulated rates of motion for the twenty site model that corresponded to the experimental temperatures. The relationship between rate (k) in s<sup>-1</sup> and activation energy in Joules is:

$$k = A e^{-E_a / (k_b T)}$$

By taking the log of both sides, a linear equation is obtained:

$$\text{Log } k = \log A - E_a / k_b (1/T)$$

The slope (m) of this line is:

$$m = - E_a / k_b$$

Therefore, the activation energy is:

$$E_a = - (k_b) (m)$$

A plot of the two simulated rates ( $9 \times 10^2 \text{ s}^{-1}$  and  $4 \times 10^3 \text{ s}^{-1}$ ) versus the inverse of the corresponding experimental temperatures ( $-60^\circ\text{C}$  and  $+100^\circ\text{C}$ , respectively) is seen in Figure 23. The slope of this line is  $-322.1$ . Thus, using the above equation, the activation energy is 4.4J.

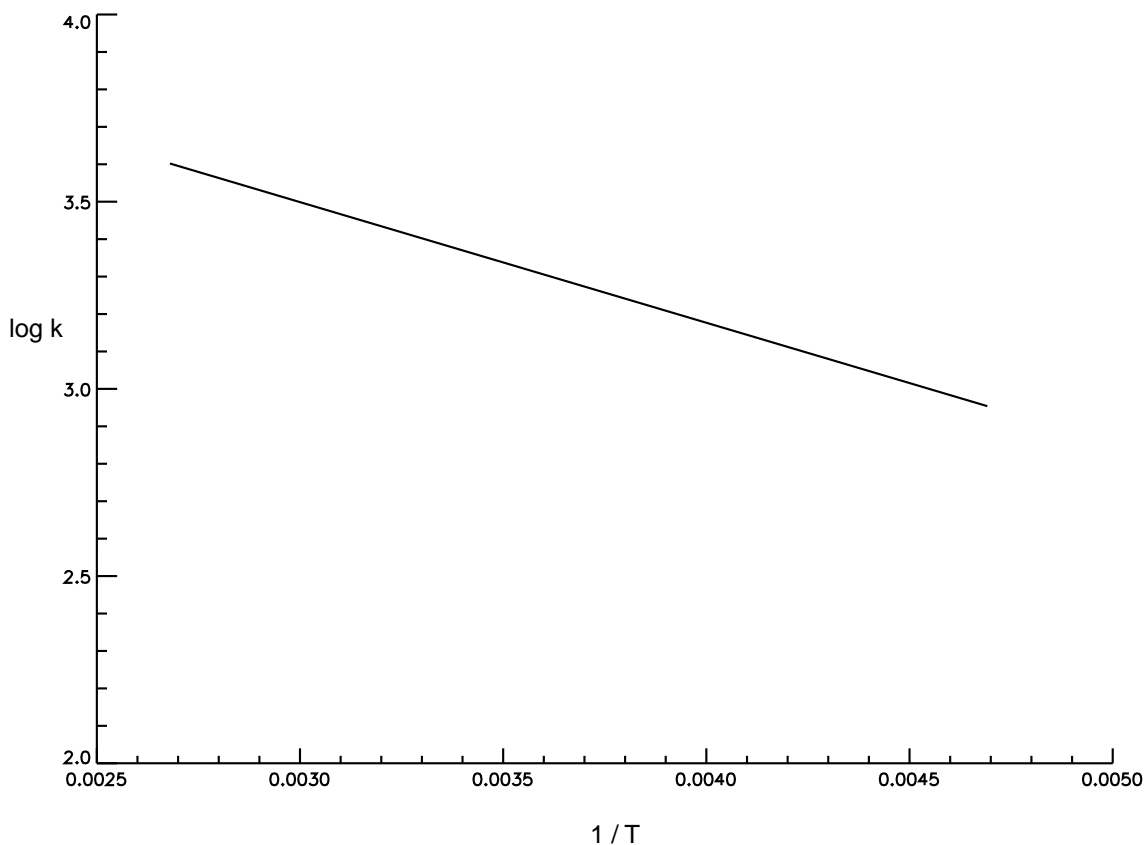


*Figure 23: Linear relationship between the log k for the simulated rates in  $s^{-1}$  and the inverse of the experimental temperatures in degrees Kelvin.*

While it is possible to obtain this estimate for the activation energy, it must be remembered that only two points were used, so this calculation needs many more data points to be accurate and reliable. The future goals of this experiment would be to match more experimental temperature spectra to simulated rates of motion to obtain a good value for the activation energy.

## VII. References

- [1] Macomber, R. S., *A Complete Introduction to Modern NMR Spectroscopy*, John Wiley and Sons, Inc., New York, 1998.
- [2] Olsen, S. C. 1997. "<sup>2</sup>H NMR Longitudinal Relaxation Studies of Polycrystalline Methyl Deuterated L-Leucine-d<sub>3</sub> and Cyclo(leucine-glycine)-d<sub>3</sub>." Honors thesis for BS in Physics, College of William and Mary.
- [3] Keniry, M. A., Kintanar, A., Smith, R. L., Gutowsky, H. S. and Oldfield, E., *Biochemistry*, **23**, 288-298, 1984.
- [4] Sanders, J. K. M., and Hunter, B. K., *Modern NMR Spectroscopy: A Guide for Chemists*, Oxford University Press, New York, 1993.
- [5] Griffiths, D. J., *Introduction to Quantum Mechanics*, Prentice Hall, New Jersey, 1995.
- [6] T. Y. Tse, "<sup>2</sup>H NMR Studies of Molecular Motion in Solids." Ph. D. Dissertation, College of William and Mary, (1994).
- [7] Hoatson, G.L., and Vold, R. L., "<sup>2</sup>H NMR Spectroscopy of Solids and Liquid Crystals." *NMR Basic Principles and Progress*, **32**, 1 (1994).